

Supplementary Information

Zeolite-supported metal complexes of rhodium and of ruthenium: a general synthesis method influenced by molecular sieving effects

Isao Ogino,^a Cong-Yan Chen,^b and Bruce C. Gates*^a

^aDepartment of Chemical Engineering and Materials Science, University of California, Davis, CA 95616, U.S.A.

^bChevron Energy Technology Co., Richmond, CA 94708, U.S.A.

Details of the EXAFS data fitting and selection of the model for the zeolite H-Beta-supported Rhodium *gem*-dicarbonyl.

The IR data indicated the formation of rhodium *gem*-dicarbonyl by two ν_{CO} bands. Thus, all models presented in Table S1 include Rh–O_{zeolite}, Rh–C, and Rh–O* contributions where the Rh–O* contribution was characterized by co-linear multiple scattering in the group Rh–C–O. The first model (Model A) is a three-shell model with these three contributions. The second model (Model B) includes an additional contribution of Rh–Rh to check for possible cluster formation resulting from reduction of the rhodium (none was found within the error of EXAFS analysis). The third model (Model C) includes a second Rh–O contribution (denoted as Rh–O_l, where the “l” subscript stands for “long”) arising from support oxygen atoms that may interact with rhodium atoms through non-covalent interaction. The fourth model (Model D) includes a Rh–Al contribution instead of a Rh–Rh contribution, because the IR data indicate the formation of rhodium *gem*-dicarbonyl at Al sites.

All of the models except Model A represented in Table S1 fit the overall data well (Figures S4 and S6). However, all of the models except D gave at least one physically unrealistic parameter value or an individual shell that is not fitted well. Therefore, these models were rejected, as summarized in Table S2 and in the following paragraphs.

Model A does not fit the data well (Figure S3), and gave fit variances larger than 1% (Table S1), leading to the rejection of Model A. Addition of a Rh–Rh contribution in Model B resulted in 50% larger goodness-of-fit value (Table S1), and it gave an unrealistically large $\Delta\sigma^2$ value ($19 \times 10^{-3} \text{ \AA}^2$) for the Rh–Rh contribution. Furthermore, the individual shell for the Rh–Rh contribution was not fit well on application of phase- and amplitude-correction; the maximum of the imaginary part of the FT was markedly offset from the maximum of the absolute magnitude of the FT (Figure S5). Thus, Model B was rejected, and we conclude that there is no evidence of cluster formation within the error of the EXAFS analysis.

Replacement of the Rh–Rh contribution with a Rh–O_l contribution (Model C) improved the fit considerably. All parameters were physically acceptable. However, the individual shell for the Rh–O_l contribution was not fit well on application of phase- and amplitude-correction (Figure S7). Thus, this model was also rejected.

In Model D, the Rh–Al contribution replaced the Rh–O_l contribution of Model C, resulting in the smallest goodness-of-fit value (Table S1) with all physically reasonable parameters. Thus, we consider that this model represent the EXAFS data the best and recommended it.

25

Details of the EXAFS data fitting and selection of the model for the zeolite H-SSZ-42-supported Rhodium *gem*-dicarbonyl.

Construction of candidate models for the EXAFS data fitting for the H-SSZ-42-supported sample was performed similarly to that for the zeolite H-Beta-supported sample. The IR data indicated the formation of rhodium *gem*-dicarbonyls. Thus, all models presented in Table S3 include Rh–O_{zeolite}, Rh–C, and Rh–O* contributions. The first model (Model A) is a three-shell model with these three contributions. To test for possible cluster formation resulting from reduction of the rhodium, Model B and D include an Rh–Rh contribution (none was found within the error of EXAFS analysis). The third model (Model C) includes a second Rh–O contribution. The Model D includes a Rh–O_l contribution in addition to a Rh–Rh contribution. Model E includes both Rh–O_l and Rh–Al contributions.

The three-shell model did not fit the data well (Figure S8) as was the case for the zeolite H-Beta-supported sample.

All of the models except Model A represented in Table S1 essentially fit the overall data well (Figures S4 and S6). However, all of the models except D gave at least one physically unrealistic parameter value or an individual shell that is not fitted well. Therefore, these models were rejected, as summarized in Table S2 and in the following paragraphs.

Model A does not fit the data well (Figure S3), and gave fit variances larger than 1% (Table S1), leading to the rejection of Model A. Addition of a Rh–Rh contribution in Model B lowered fit variances below 1% but increased goodness-of-fit value considerably (Table S3); the individual shell for the Rh–Rh contribution was not fit well on application of phase- and amplitude-correction; the maximum of the imaginary part of the FT was markedly offset from the maximum of the absolute magnitude of the FT (Figure S10). Thus, Model B was rejected, and we conclude that there is no evidence of cluster formation within the error of the EXAFS analysis.

Replacement of the Rh–Rh contribution with a Rh–Al contribution (Model C) improved the fit considerably (Figure S11). However, this model gave unrealistically large ΔE_0 value (-17 eV) for the Rh–Al contribution, and the individual shell for the Rh–Al contribution was not fit well on application of phase- and amplitude-correction (Figure S12). Thus, this model was also rejected.

Replacement of the Rh–Al contribution with a Rh–O_l contribution in Model D did not improve the fit (Figure S13); ΔE_0 values for the Rh–C, Rh–O_l, Rh–Rh contributions were relatively large (Table S3), and the individual shell for the Rh–Rh contribution was not fit well on application of phase- and amplitude-correction (Figure S14), leading to the rejection of this model.

In Model E, the Rh–Al contribution replaced the Rh–Rh contribution of Model D, resulting in the smallest goodness-of-fit value (Table S3) with all physically reasonable parameters. Thus, we consider that this model represent the EXAFS data the best and recommended it.

Table S1. EXAFS parameters corresponding to four candidate models characterizing the zeolite H-Beta-supported rhodium *gem*-dicarbonyl.

model	backscatterer	<i>N</i>	$10^3 \Delta\sigma^2 (\text{\AA}^2)$	<i>R</i> (\text{\AA})	ΔE_0 (eV)	fit variances		ε_v^2
						Abs	Im	
A	O	2.5	4.3	2.13	-3.4			
	C	2.3	3.4	1.83	4.3	0.49	1.9	29
	O*	2.5	3.3	2.99	-4.5			
B	O	2.4	4.0	2.13	-3.6			
	C	2.2	3.0	1.83	4.2	0.29	1.3	43
	O*	2.2	2.0	2.99	4.6			
	Rh	1.1	5.5	3.13	-19			
C	O	2.1	3.2	2.13	-2.3			
	C	1.9	2.4	1.83	4.2	0.20	0.47	29
	O*	2.1	2.5	2.98	-2.0			
	O _l	1.5	1.1	3.19	-2.6			
D	O	2.2	3.4	2.12	-1.7			
	C	2.0	2.8	1.83	4.5	0.18	0.43	14
	O*	2.0	2.7	2.97	-1.1			
	Al	1.2	4.7	3.08	-5.0			

^aFit details: *R*-space, $2.14 < k < 14.95 \text{ \AA}^{-1}$ and $0.5 < R < 3.0 \text{ \AA}$. Notation: *N*, coordination number; *R*, inter-atomic distance; $\Delta\sigma^2$, Debye–Waller parameter (sigma-squared parameter); ΔE_0 , inner potential correction; Abs, absolute part of the k^2 -weighted FT; Im., imaginary part of the k^2 -weighted FT; ε_v^2 , goodness of fit.

Table S2. Qualitative summary of EXAFS fitting results for four candidate models representing the zeolite H-Beta-supported rhodium gem-dicarbonyl.

model	absorber/backscatterer contribution	comments regarding quality of fit of EXAFS data to the model
A	Rh–O Rh–C Rh–O*	too large fit variance; data not fitted well
B	Rh–O Rh–C Rh–O* Rh–Rh	worst goodness-of-fit value; unrealistically large $\Delta\sigma^2$ value ($-19 \times 10^{-3} \text{ \AA}^2$) of the Rh–Rh contribution; individual Rh–Rh shell not fit well when phase- and amplitude-corrections applied
C	Rh–O Rh–C Rh–O* Rh–O _l	individual Rh–O _l shell not fit well when phase- and amplitude-corrections applied
D	Rh–O Rh–C Rh–O* Rh–Al	smallest goodness-of-fit value; good overall fit with physically realistic parameters

Table S3. EXAFS parameters corresponding to four candidate models characterizing the SSZ-42-supported rhodium gem-dicarbonyls.

model	backscatterer	<i>N</i>	$10^3 \Delta\sigma^2 (\text{\AA}^2)$	<i>R</i> (\text{\AA})	ΔE_0 (eV)	fit variances		ε_v^2
						Abs	Im.	
A	O	1.9	3.5	2.09	-1.6			
	C	1.9	3.1	1.82	9.0	0.77	2.5	24
	O*	1.9	2.8	2.99	-1.3			
B	O	1.8	3.2	2.08	-1.2			
	C	1.8	3.1	1.82	8.7			
	O*	1.8	2.7	2.97	0.62	0.32	0.92	34
	Rh	1.1	9.1	2.99	11			
C	O	1.9	3.3	2.08	-0.85			
	C	1.9	3.2	1.82	8.8			
	O*	1.9	2.7	2.99	-0.73	0.43	0.95	15
	Al	1.3	9.7	3.27	-17			
D	O	1.8	2.9	2.08	1.5			
	C	1.9	3.6	1.82	12			
	O*	1.9	2.9	2.96	3.4	0.36	0.78	13
	O _l	0.78	5.5	2.46	11			
	Rh	1.2	7.7	2.99	10			
E	O	1.9	3.3	2.08	0.4			
	C	1.9	3.2	1.82	9.8			
	O*	1.9	2.9	2.98	1.6	0.21	0.56	12
	O _l	0.41	2.5	2.46	1.6			
	Al	0.73	4.9	3.15	-9.7			

^aFit details: *R*-space, $2.19 < k < 16.82 \text{ \AA}^{-1}$; $0.5 < R < 2.9 \text{ \AA}$. Notation: *N*, coordination number; *R*, inter-atomic distance; $\Delta\sigma^2$, Debye–Waller parameter (sigma-squared parameter); ΔE_0 , inner potential correction; Abs, absolute part of the k^2 -weighted FT; Im., imaginary part of the k^2 -weighted FT; ε_v^2 , goodness of fit.

Table S4. Qualitative summary of EXAFS fitting results for five candidate models representing the zeolite H-SSZ-42-supported rhodium *gem*-dicarbonyls.

model	absorber/backscatterer contribution	comments regarding quality of fit of EXAFS data to the model
A	Rh–O Rh–C Rh–O*	too-large fit variance; data are not fitted well
B	Rh–O Rh–C Rh–O* Rh–Rh	worst goodness-of-fit value; individual Rh–Rh shell not fitted well when phase- and amplitude-corrections applied
C	Rh–O Rh–C Rh–O* Rh–Al	unrealistically large ΔE_0 value (-17 eV) of Rh–Al contribution; individual Rh–Al shell not fitted well when phase- and amplitude-corrections applied
D	Rh–O Rh–C Rh–O* Rh–O _l Rh–Rh	relatively large ΔE_0 values of the Rh–C and Rh–O _l contributions; individual Rh–Rh shell not fitted well when phase- and amplitude-corrections applied
E	Rh–O Rh–C Rh–O* Rh–O _l Rh–Al	smallest goodness-of-fit value; good overall fit with physically realistic parameters

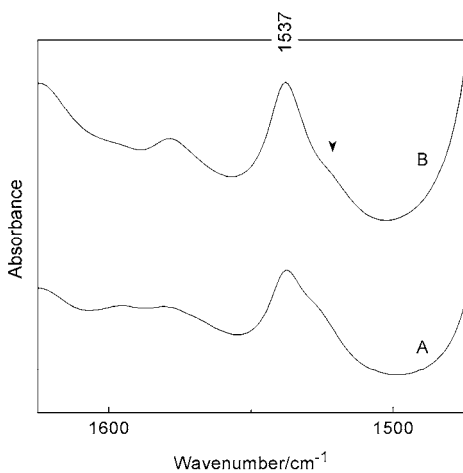


Figure S1. IR spectra in the region 1500–1600 cm⁻¹ characterizing zeolite-supported samples formed from the reaction of **IV** with H-SSZ-42-zeolite in *n*-pentane for (A) 1 day and (B) 4 days. The arrow indicates the reduction of the absorbance characteristic of acac ligands bonded to Rh atoms.

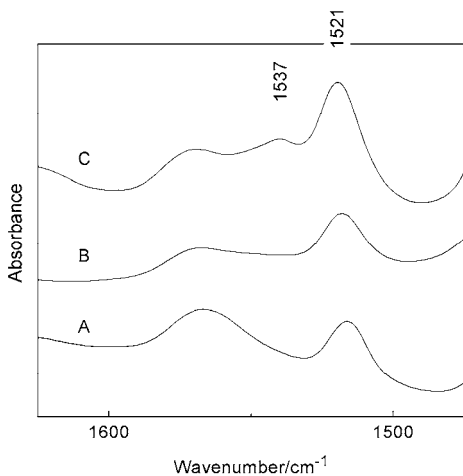


Figure S2. IR spectra in the region 1500–1600 cm⁻¹ characterizing zeolite-supported ruthenium complexes formed from the reaction of **III** with various zeolites: (A) H-SSZ-42, (B) H-Mordenite, and (C) ZSM-5.

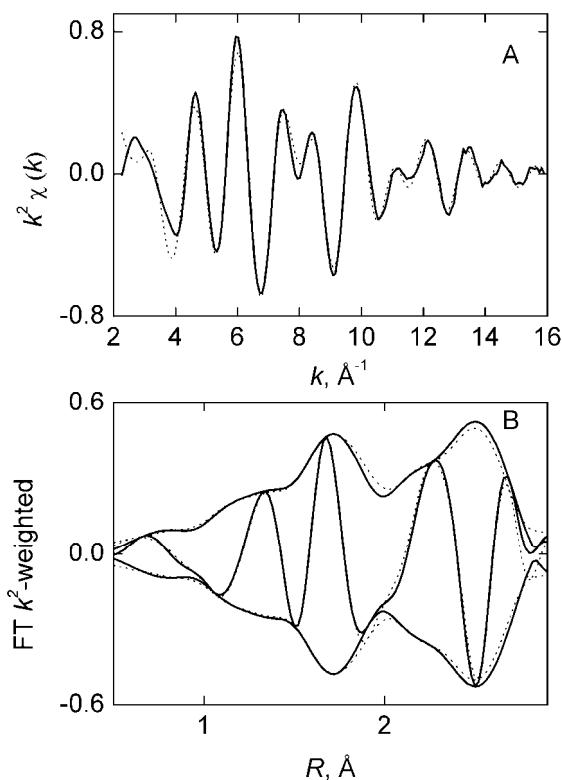


Figure S3. Results of EXAFS analysis for zeolite H-Beta-supported rhodium *gem*-dicarbonyl formed by the reaction of **IV** with the zeolite according to Model A: (A) k^2 -Weighted EXAFS data (solid line) and the best fit (dotted line). (B) Magnitude and imaginary part of Fourier transform of k^2 -weighted EXAFS data (solid lines) and the best fit (dotted lines). Fit range: $2.28 < k < 15.95 \text{ \AA}^{-1}$; $0.5 < R < 2.9 \text{ \AA}$.

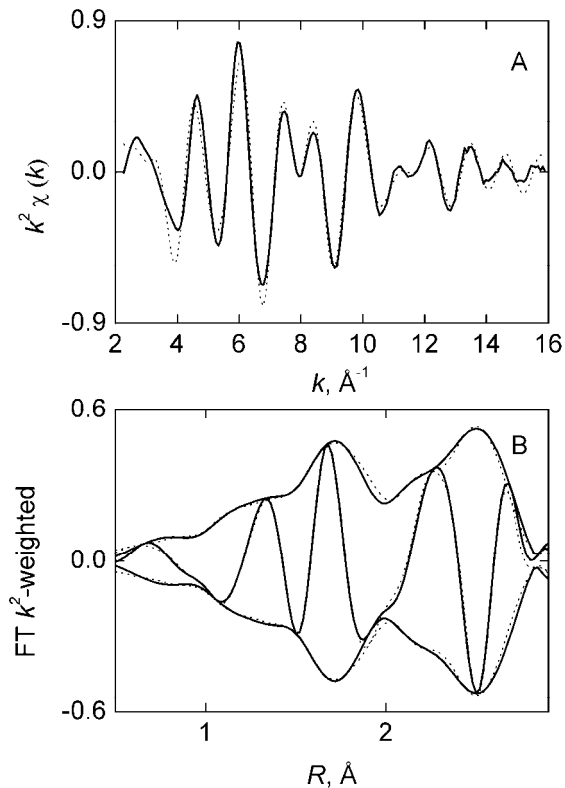


Figure S4. Results of EXAFS analysis for zeolite H-Beta-supported rhodium *gem*-dicarbonyl formed by the reaction of **IV** with the zeolite according to Model **B**: (A) k^2 -Weighted EXAFS data (solid line) and the best fit (dotted line). (B) Magnitude and imaginary part of Fourier transform of k^2 -weighted EXAFS data (solid lines) and the best fit (dotted lines). Fit range: $2.28 < k < 15.95 \text{ Å}^{-1}$; $0.5 < R < 2.9 \text{ Å}$.

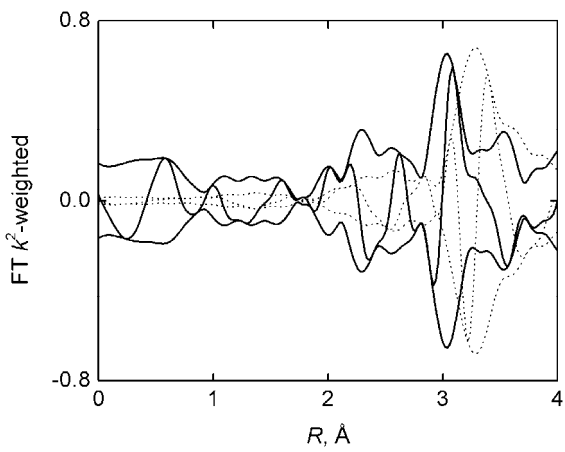


Figure S5. Results of EXAFS data analysis for the zeolite H-Beta-supported rhodium *gem*-dicarbonyl according to Model **B**: Rh–Rh phase- and amplitude-corrected k^2 -weighted Fourier transform of the difference spectrum (solid line) and fit (dotted line) representing Rh–Rh contribution to the EXAFS data.

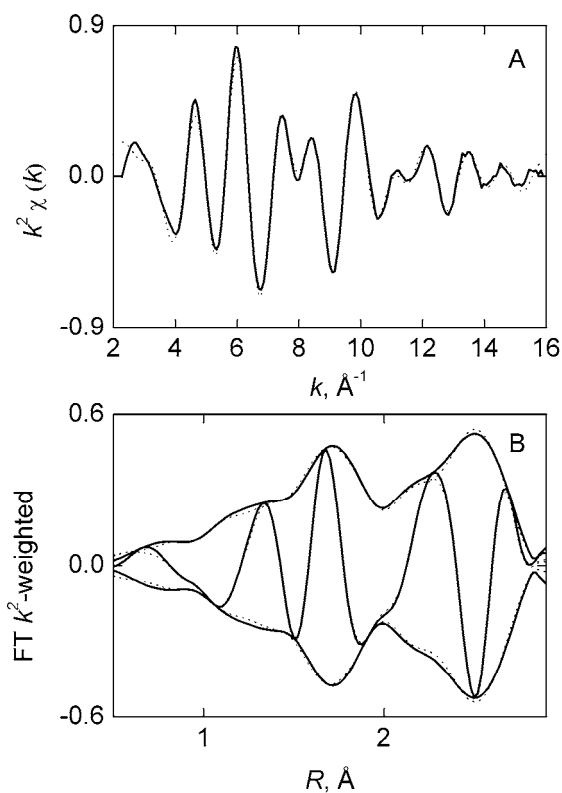


Figure S6. Results of EXAFS analysis for zeolite H-Beta-supported rhodium *gem*-dicarbonyl formed by the reaction of **IV** with the zeolite according to Model C: (A) k^2 -Weighted EXAFS data (solid line) and the best fit (dotted line). (B) Magnitude and imaginary part of Fourier transform of k^2 -weighted EXAFS data (solid lines) and the best fit (dotted lines). Fit range: $2.28 < k < 15.95 \text{ Å}^{-1}$; $0.5 < R < 2.9 \text{ Å}$.

5

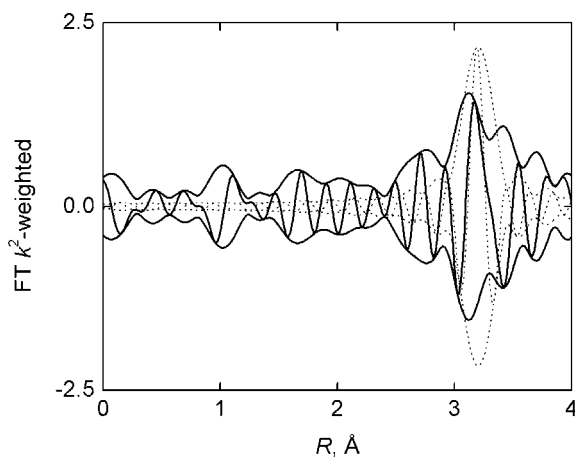


Figure S7. Results of EXAFS data analysis for the zeolite H-Beta-supported rhodium *gem*-dicarbonyl according to Model C: Rh–O₁ phase- and amplitude-corrected k^2 -weighted Fourier transform of the difference spectrum (solid line) and fit (dotted line) representing Rh–Rh contribution to the EXAFS data.

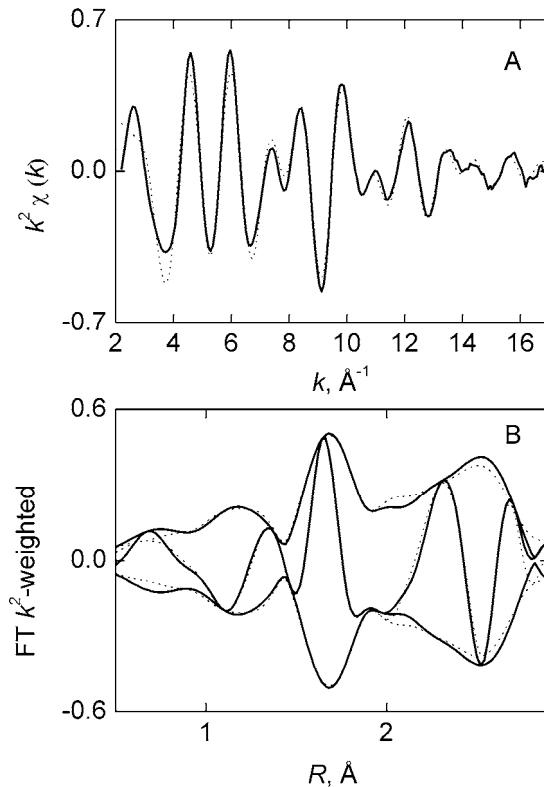


Figure S8. Results of EXAFS analysis for zeolite H-SSZ-42-supported rhodium *gem*-dicarbonyls formed by the reaction of **IV** with the zeolite according to Model A: (A) k^2 -Weighted EXAFS data (solid line) and the best fit (dotted line). (B) Magnitude and imaginary part of Fourier transform of k^2 -weighted EXAFS data (solid lines) and the best fit (dotted lines). Fit range: $2.19 < k < 16.82 \text{\AA}^{-1}$; $0.5 < R < 2.9 \text{\AA}$.

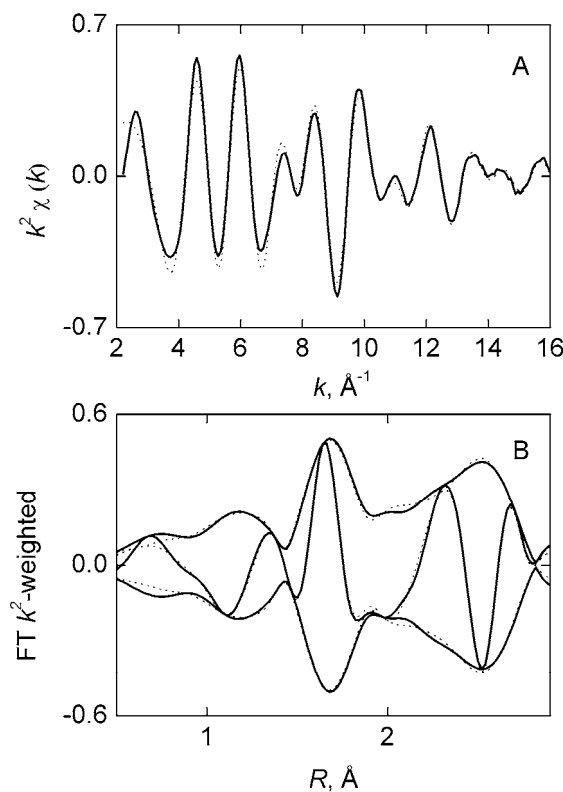


Figure S9. Results of EXAFS analysis for zeolite H-SSZ-42-supported rhodium *gem*-dicarbonyls formed by the reaction of **IV** with the zeolite according to Model **B**: (A) k^2 -Weighted EXAFS data (solid line) and the best fit (dotted line). (B) Magnitude and imaginary part of Fourier transform of k^2 -weighted EXAFS data (solid lines) and the best fit (dotted lines). Fit range: $2.19 < k < 16.82 \text{ Å}^{-1}$; $0.5 < R < 2.9 \text{ Å}$.

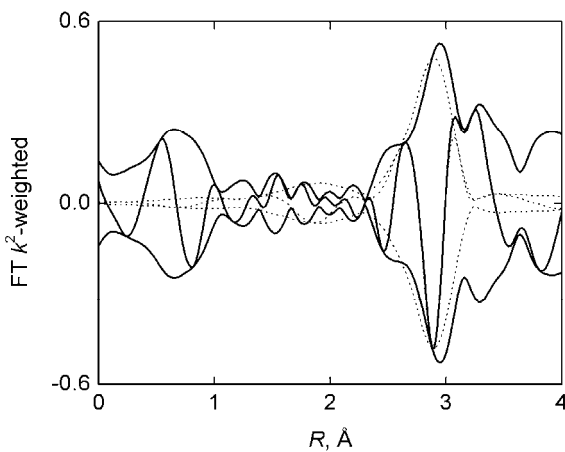


Figure S10. Results of EXAFS data analysis for the zeolite H-SSZ-42-supported rhodium *gem*-dicarbonyl according to Model **B**: Rh–O₁ phase- and amplitude-corrected k^2 -weighted Fourier transform of the difference spectrum (solid line) and fit (dotted line) representing Rh–Rh contribution to the EXAFS data.

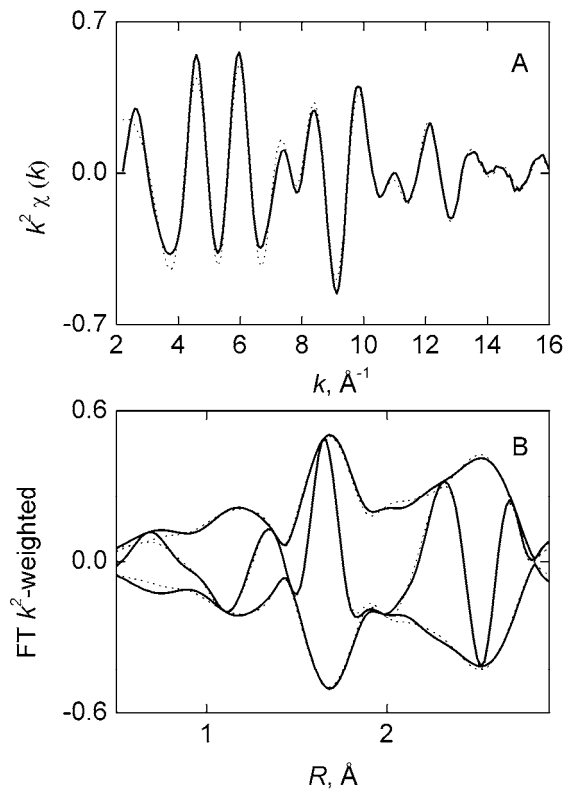


Figure S11. Results of EXAFS analysis for zeolite H-SSZ-42-supported rhodium *gem*-dicarbonyls formed by the reaction of **IV** with the zeolite according to Model C: (A) k^2 -Weighted EXAFS data (solid line) and the best fit (dotted line). (B) Magnitude and imaginary part of Fourier transform of k^2 -weighted EXAFS data (solid lines) and the best fit (dotted lines). Fit range: $2.19 < k < 16.82 \text{ \AA}^{-1}$; $0.5 < R < 2.9 \text{ \AA}$.

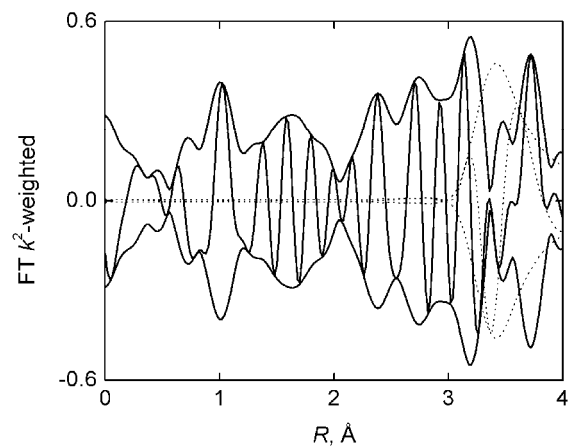


Figure S12. Results of EXAFS data analysis for the zeolite H-SSZ-42-supported rhodium *gem*-dicarbonyl according to Model C: Rh–O₁ phase- and amplitude-corrected k^2 -weighted Fourier transform of the difference spectrum (solid line) and fit (dotted line) representing Rh–Rh contribution to the EXAFS data.

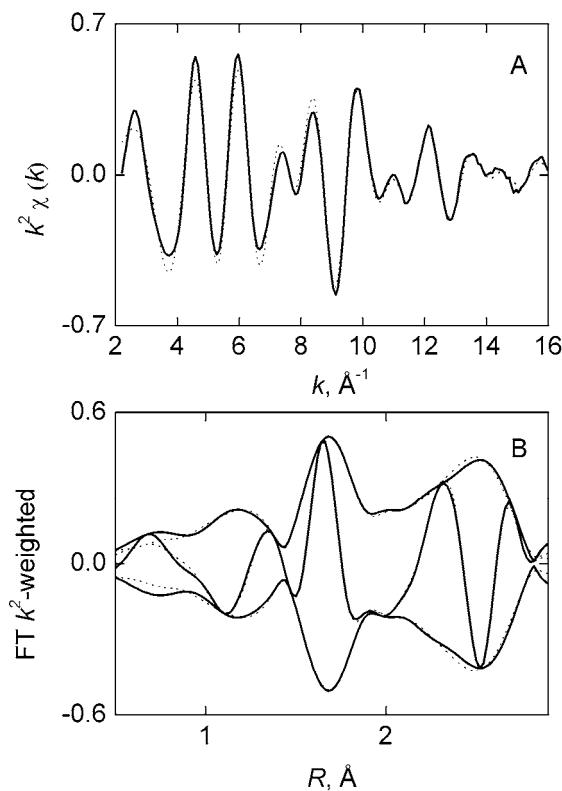


Figure S13. Results of EXAFS analysis for zeolite H-SSZ-42-supported rhodium *gem*-dicarbonyls formed by the reaction of **IV** with the zeolite according to Model **D**: (A) k^2 -Weighted EXAFS data (solid line) and the best fit (dotted line). (B) Magnitude and imaginary part of Fourier transform of k^2 -weighted EXAFS data (solid lines) and the best fit (dotted lines). Fit range: $2.19 < k < 16.82 \text{ Å}^{-1}$; $0.5 < R < 2.9 \text{ Å}$.

5

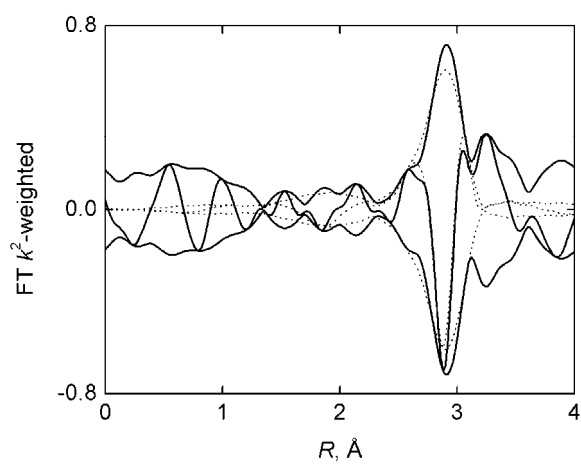


Figure S14. Results of EXAFS data analysis for the zeolite H-SSZ-42-supported rhodium *gem*-dicarbonyl according to Model **D**: Rh–O₁ phase- and amplitude-corrected k^2 -weighted Fourier transform of the difference spectrum (solid line) and fit (dotted line) representing Rh–Rh contribution to the EXAFS data.